THE JOURNAL OF PHYSICAL CHEMISTRY C

pubs.acs.org/JPCC Article

Temperature Effects on CO_2 Electroreduction Pathways in an Imidazolium-Based Ionic Liquid on Pt Electrode

Tianrong Zhan, Anil Kumar, Michael Sevilla, Arun Sridhar, and Xiangqun Zeng*

Cite This: J. Phys. Chem. C 2020, 124, 26094−26105 Read Online

ACCESS | Metrics & More | Article Recommendations | Supporting Information

ABSTRACT: Ionic liquids (ILs) are thermally stable at both high and low temperatures, making them excellent solvents and electrolytes in extreme ambient conditions. In this work, we systematically studied the temperature effects on the various pathways of electrochemical reduction of CO_2 in 1-ethyl-3-methylimidazolium bis(trifluoromethylsulfonyl)imide ([Emim][NTf_2]) and compared them with those in 1-butyl-1-methylpyrrolidinium bis(trifluoromethylsulfonyl)imide ([Bmpy][NTf_2]) by electrochemical methods and density functional calculations. We summarize the crucial factors determining the reaction pathways for electroreduction of CO_2 in [Emim][NTf_2]. Our results show that temperature can be used to modulate the reaction pathway of electrochemical reduction of carbon dioxide in this imidazolium-based IL via the effects on (i) the mass transport of the reactant and intermediates, (ii) the adsorption and solubility of the intermediates species, and (iii) the IL−electrode interface structure and properties.

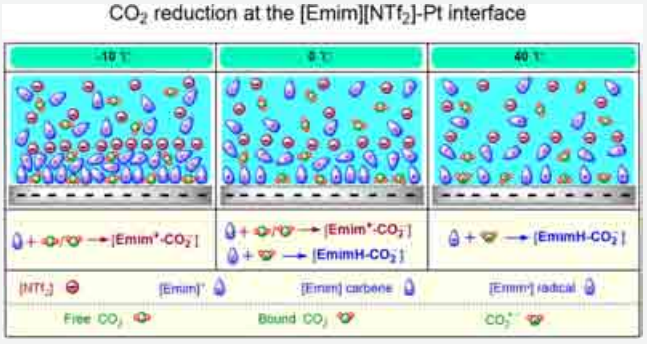

INTRODUCTION

The increasing need for clean energy sources has driven renewed interest in developing greener methods for both energy production and value-added chemical synthesis.[1,2] The abundance of CO_2 in the atmosphere and the detrimental greenhouse effects of CO_2 on our environment and climates motivate significant research efforts toward understanding the mechanisms of the electrochemical reduction of CO_2 in order to facilitate the development of electrochemical systems for the conversion of CO_2 to useful fuels and chemicals. Electroreduction of CO_2 has sluggish kinetics since the first one-electron reduction step to form $CO_2^{\bullet-}$, as eq 1 needs a relatively high reduction potential of −1.9 V vs normal hydrogen electrode (NHE).[3] Consequently, many efforts have been devoted to developing highly efficient catalysts and supporting electrolytes to lower the overpotential and to control the pathway of CO_2 electroreduction.[4−9]

$$CO_2 + e^- \rightarrow CO_2^{\bullet-} \quad (1)$$

Ionic liquids (ILs) have good thermal and chemical stability, a wide electrochemical window, and negligible volatility, which make them "green" solvents and electrolytes to replace traditional toxic and volatile organic solvents. IL can also act as electron transfer mediators in many electrochemical processes.[10,11] Combined with their high solubility of CO_2 and strong ability to stabilize the charged CO_2 species, ILs are among the most promising materials for promotion for electrochemical reduction of CO_2.[6,12−14] Since Rosen's group reported that the addition of 1-ethyl-3-methylimidazolium tetrafluoroborate ([Emim][BF_4]) to the electrolyte can significantly lower the overpotential of CO_2 reduction on the Pt electrode,[15] this beneficial effect of imidazolium-based IL has been verified in numerous subsequent studies by combining with different electrode materials such as Ag,[16] Pb,[13] Sn,[17] Bi,[18] Cu,[7] and Pt.[19] More recently, Cuesta's group summarized different mechanisms accounting for the reduced CO_2 reduction overpotentials in the imidazolium-based IL system.[20] Rosen et al. addressed that the lowered overpotential was attributable to the stabilization of the $CO_2^{\bullet-}$ intermediate via coupling with the electrogenerated imidazolium carbene at the 2-position.[15] Other researchers advised the formation of [Emim$^{\bullet}$] radical−$CO_2^{\bullet-}$ adduct ([EmimH−CO_2^-]) through radical−radical coupling between the [Emim$^{\bullet}$] radical (rather than the carbene) and $CO_2^{\bullet-}$.[19,21] The operando spectroscopic results in Braunschweig's report instead suggested that C2-carboxylic acid complex plays a significant role in the reduction of CO_2 to CO and formate on Pt electrodes.[22] Nevertheless, these prior reports from various groups have not yet fully elucidated the catalytic mechanisms of these types of

Received: July 2, 2020
Revised: October 26, 2020
Published: November 23, 2020

https://dx.doi.org/10.1021/acs.jpcc.0c06065
J. Phys. Chem. C 2020, 124, 26094−26105

imidazolium-featured promoters; the main conclusion indicates that the use of imidazolium-based IL could reduce the CO_2 reduction overpotential, inhibit the hydrogen evolution reaction (HER), and improve the selectivity of reduction products.[23−28] Though the complexation between the $CO_2^{\bullet-}$ and the $[Emim]^+$ cation would lower activation energy,[15] clear cation effects on CO_2 electroreduction reveal that the formation of an imidazolium cation−$CO_2^{\bullet-}$ complex is impossible after an initial, rate-determining reduction step.[29] The more acceptable mechanisms are the formation of imidazolium radical−$CO_2^{\bullet-}$ complex through a radical−radical coupling and the formation of imidazolium carbene−CO_2 adduct through a coupling reaction between carbene and CO_2 molecules. The electrochemical reduction of CO_2-saturated imidazolium-based IL generally results in the main product of CO, but the catalytic pathway and products are also highly dependent on the surface structure of the electrode.[13] It is well established that CO_2 interacts with the metallic electrode surface in the imidazolium-based IL electrolytes. Because of their well-structured surface, single-crystal electrodes are regarded as the most convenient candidates for the investigation of electrocatalytic processes in ILs. For example, the experimental and density functional theory (DFT) studies in Nakamura's work underscore the significance of the reduced $[Emim]^+$ cation layer on the highly ordered Cu (111) electrode surface for activating CO_2.[7] Impressively, the surface-sensitive electrochemical CO_2 reduction of Hanc−Scherer's study demonstrates the formation of an electroactive adduct of [EmimH−CO_2^-] through a radical−radical coupling reaction on Pt (110) and Pt (100), while an electroinactive adduct [$Emim^+$−CO_2^-] of imidazolium carbene with CO_2 is formed on Pt (111).[19] Despite the simplicity of the single-crystal electrodes, they are not practical electrode materials due to their high-cost and sensitive surfaces at ambient conditions.

The fundamental physicochemical properties of IL are very important in determining their application potential in a given field. For electrocatalytic applications, viscosities and conductivities of IL are undoubtedly important parameters that are highly temperature-dependent.[30] Furthermore, molecular interactions such as van der Waal force and hydrogen bonding forces are abundant in the IL system. These interaction and their resultant molecular ion orientations are strongly temperature-dependent. The long-range molecular interactions can alter the physical and chemical properties of the IL. These physicochemical properties of ILs are temperature dependent. But to the best of our knowledge, the electrochemical reduction of CO_2 at different temperatures in hydrophobic IL medium has not been reported yet. There are both fundamental and applied significance to studying CO_2 reduction in the ILs at a wide temperature range. In contrast to traditional aqueous and nonaqueous solvents and electrolytes, ILs have superior thermal stabilities. Hence, they do not dry out (evaporate) at high temperatures or freeze at a low temperature, allowing them to function at extreme ambient temperature conditions. For example, there is a significant need to monitor greenhouse gas emission in Arctic Tundra and sensors based on ILs can work at the extreme environment in the Arctic region (e.g., −30 °C in winter and 10 °C in summer in northern Alaska). IL-based energy storage devices will also function better in subzero winter temperatures. The present work aims to investigate for the first time the controlling function of the temperature on the electrochemical chemical reduction of CO_2 in imidazolium-based IL. To this end, we systematically studied the electrochemical reduction of CO_2 in the IL 1-ethyl-3-methylimidazolium bis(trifluoromethylsulfonyl)imide ([Emim][NTf_2], shown in Figure 1) at different temperatures. We also use the non-

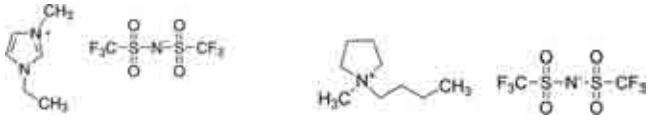

Figure 1. Molecular structures of [Emim][NTf_2] (left) and [Bmpy][NTf_2] (right).

imidazolium-based IL 1-butyl-1-methylpyrrolidinium bis(trifluoromethylsulfonyl)imide ([Bmpy][NTf_2] shown in Figure 1) as a control. Although these hydrophobic ILs are polar, trace water is inevitably present in the IL electrolyte. As shown in Table S1, we selected low-viscosity, high-conductivity, and hydrophobic [Emim][NTf_2] and [Bmpy][NTf_2] in comparison to those hydrophilic ILs, i.e., [Bmim][BF_4], [Emim][DCA], and [Emim][BF_4] previous researchers used.[31] The hydrophobicity of [Emim][NTf_2] allows water to be only at trace level (300−500 ppm)[32] and minimized the effects of water. We studied the water effect on CO_2 reduction mechanisms in [Emim][NTf_2] at the Pt electrode under both subzero and common ambient temperature range. Pt was selected as the electrode material. Compared to other metal catalysts, Pt as a catalyst for CO_2 reduction is not extensively studied since it is less active toward CO_2 reduction reaction due to competing HER and product CO poison at Pt surface. However, HER will be suppressed and CO is likely the major product at Pt electrode in hydrophobic ILs. DFT calculations were employed to verify our hypothesis and experimental observations. Specifically, we aim to determine whether and how the temperature affects the electrochemical reduction pathway of CO_2 in the [Emim][NTf_2] medium.

EXPERIMENTAL SECTION

Reagents. [Emim][NTf_2] (99%) and [Bmpy][NTf_2] (99%) were purchased from IoLiTec Inc. Their melting points are −15 and −18 °C, respectively. Different batches of the ILs could contain different amounts of trace water. High-purity gases (nitrogen, 99.99%; carbon dioxide, 99.99%) were obtained from Airgas Great Lakes (Independence, OH) and Praxair, respectively.

Electrochemistry. A one-compartment electrochemical glass cell with a three-electrode configuration was used for this study as shown in Figures S1 and S2. All cyclic voltammetry (CV) measurements were conducted by using this three-electrode cell at different temperatures on a computer-controlled CHI 700D workstation. A polycrystalline platinum disk electrode (CHI102 with a diameter of 2 mm) was used as a working electrode. This Pt disk electrode active area was determined to be 0.158 cm^2 via traditional hydrogen adsorption experiments in 0.5 M H_2SO_4 electrolyte following the literature.[33] The current density in CV results was obtained with this Pt disk electrode area. A platinum wire (1.0 mm diameter) was used as a counter electrode, and a silver wire (0.25 mm diameter) was used as a reference electrode. Ag wire is selected here mainly because of the concern that CO_2 reduction could form CO that may have a possibility to be adsorbed on the Pt quasi reference electrode. In contrast to the 0.1 M tetraethylammonium perchlorate acetonitrile−water

https://dx.doi.org/10.1021/acs.jpcc.0c06065
J. Phys. Chem. C 2020, 124, 26094−26105

mixtures used in Tomita et al.'s work that observed Ag deposit on the Ag electrode,[34] [Emim][NTf_2] is more inert and Ag wire corrosion in [Emim][NTf_2] to form Ag^+ is very unlikely. We have performed the potential calibration with ferrocene. At subzero temperature, the redox process of ferrocene/ferrocenium (Fc/Fc^+) becomes less reversible showing as a large peak potential separation (see Table S2). Thus, calibration of the electrode potential with E_0 of Fc/Fc^+ has different uncertainty at different temperature with large uncertainty at subzero temperature. This work focused on studying the temperature effects on the CO_2 reduction processes. Comparison of CV curves at varying temperature using experimental data in which electrode potential is referenced with Ag quasi reference electrode will provide more accurate information. Thus, in all CVs here, the electrode potentials are referenced with the Ag quasi reference electrode. The detailed potential calibration shown in Table S2 can be used to easily calibrate the potential and compare with literature data. The electrochemical measurements were conducted in CO_2- or N_2-saturated supporting electrolyte of either [Emim][NTf_2] or [Bmpy][NTf_2] IL. Prior to each test, the electrochemical cell was dried in hot air and N_2 gas flowed into the empty cell to remove any trace of water. Subsequently, a small volume of [Emim][NTf_2] or [Bmpy][NTf_2] (~1.0 mL) was pipetted into the cell, and then N_2 or CO_2 was purged to saturate the electrolyte for at least 30 min before each experiment. The CV experiments were performed under different potential windows at varying temperatures of −10, −5, 0, 25, and 40 °C using a scan rate of 100 mV s^{-1}. The gas flow rate was controlled at 30 sccm (standard cubic centimeters per minute) by using MKS (MKS Instruments, Inc.) type 247 four-channel readout (bundled with Mass-Flo controller). The temperature was controlled to accuracy of ±1 °C by our homemade controller as described in Supporting Information and Figure S2.

Computational Study. The B3LYP density functional implemented in the Gaussian 16 suite of programs[35] was used to compute the energetics and thermodynamics of reactions at 298 K including the effect of the IL environment (ε = 11.7) by use of the integral equation formalism of the polarized continuum model (IEF-PCM)[36] All structures were fully optimized using the 6-31++G** basis set, and thermodynamic energies (free energy (G), enthalpy (H), and entropy (S)) at 298 K were evaluated via vibrational analysis. For all the optimized structures, positive frequencies were achieved that ensure the stable minimum structure for the molecules in question. Detailed computational calculation results are shown in the Supporting Information.

RESULTS AND DISCUSSION

1. Cyclic Voltammetry of [Emim][NTf_2] with and without CO_2 at Varying Temperature. It has been extensively proven that [Emim][NTf_2] is highly stable in a wide potential window. However, in the absence of any other electroactive species, the $[Emim]^+$ cation may be electrochemically reduced to the corresponding [Emim$^\bullet$] radicals as shown in eq 2.[37] Thus, the electrochemical stability of the $[Emim]^+$ cation governs its cathodic polarization window. Figure 2 displays the CV curves of [Emim][NTf_2] between −1.3 and 1.0 V at room temperature (25 °C). In this potential window, CO_2 cannot be reduced and the oxidation of $[NTf_2]^-$ anions is negligible, allowing us to study the redox behavior of $[Emim]^+$ cations. Poor reversibility of redox behaviors are

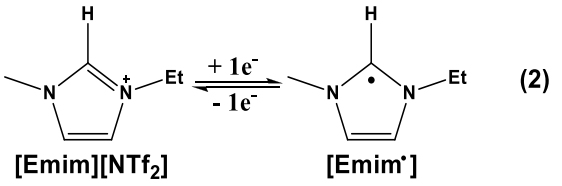

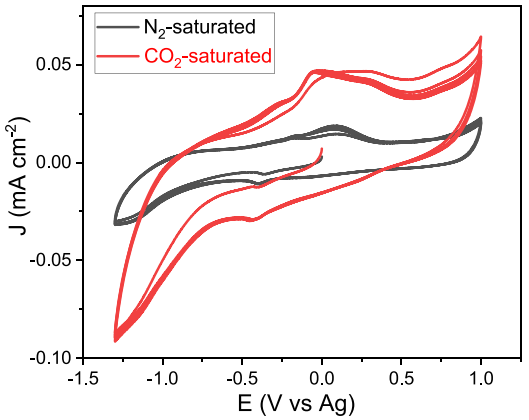

Figure 2. CVs in the potential range from 1 to −1.3 V in CO_2- and N_2-saturated [Emim][NTf_2].

observed on Pt polycrystalline electrode in both N_2- and CO_2-saturated electrolytes, and this mainly results from the presence of impurities such as trace water. The effect of water was studied and discussed in the later section. Nevertheless, we explicitly found the oxidative response of [Emim$^\bullet$] radicals back to the initial cations, supporting the high stability of the formed imidazolium radicals. Similar well-defined quasi-reversible voltammetric responses on the Pt(111) electrode were already recorded in other imidazolium-based IL systems.[19,38] However, despite similar CV curve shapes, the larger voltammetric response under a CO_2 atmosphere in [Emim][NTf_2] implies the presence of relatively strong interactions between [Emim][NTf_2] and CO_2.

To investigate the temperature effects, we examined the CV curves in N_2-saturated [Emim][NTf_2] by extending the cathodic potential limit up to −3.1 V at various temperatures in the range of −10 to 40 °C (Figure 3a). In this potential window, the reduction of both CO_2 and proton is expected to take place. Impressively, the slightly reversible electrode reaction related to $[Emim]^+/[Emim^\bullet]$ radical formation disappears at all tested temperatures in this wide potential window. Instead, all CV curves exhibit the new reduction processes at more negative cathodic onset potentials (E_0, for convenience, taking the potential at a current density of 190 μA cm^{-2} as onset potential) between −1.3 and −2.0 V. This process has been already recognized as the electrochemical reduction of the imidazolium cation to carbene accompanying HER as shown in eq 3 and supported by early literature

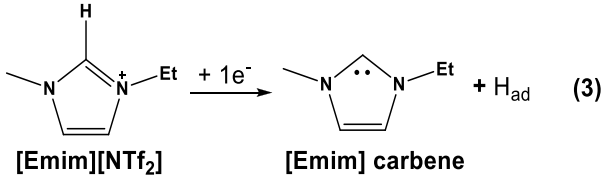

reports.[19,38] Since Pt electrode can produce in nonaqueous electrolytes strong HER albeit at very low water concen-

https://dx.doi.org/10.1021/acs.jpcc.0c06065
J. Phys. Chem. C 2020, 124, 26094−26105

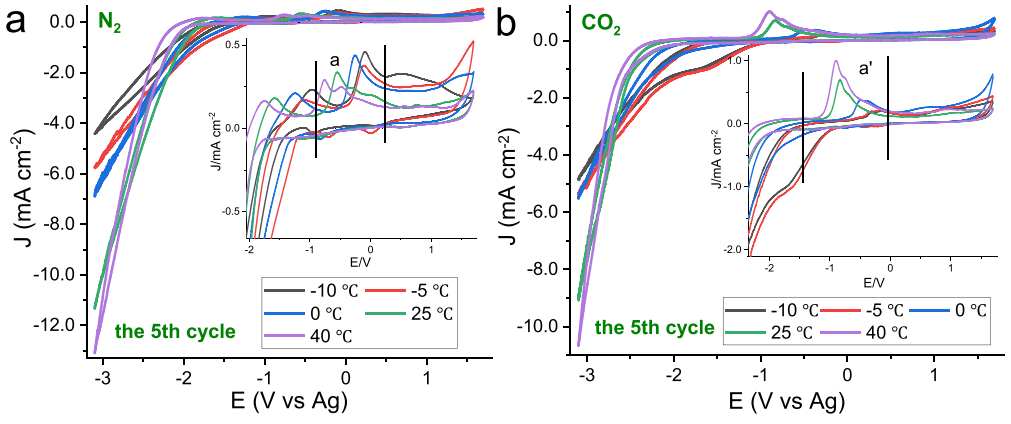

Figure 3. CV curves (the fifth cycle) of Pt in N_2- and CO_2-saturated [Emim][NTf_2] in the potential range from −3.1 to 1.7 V.

trations,[31] the cathodic sweeps exhibit the combined response of the competitive reduction reactions between the reduction of imidazolium cations and HER. In the subsequent anodic scan, oxidation of the newly electrogenerated H_2 can be distinctly seen in all curves (inset of Figure 3a, oxidation peaks between −0.9 and −2.0 V). By comparison, the oxidation peaks at a potential range between −0.09 and −0.76 V have been already assigned to the oxidation of the newly formed imidazolium carbene back to the initial cation.[39] Also, the above observations demonstrate that the oxidation signals of hydrogen are overtly smaller than those of imidazolium carbene species being oxidized back to their initial cations. This fact revealed that HER on the Pt electrode was suppressed in [Emim][NTf_2] electrolyte with a very low water concentration.[22]

For comparison, the CV curves in CO_2-saturated [Emim][NTf_2] were also obtained under the same conditions shown in Figure 3b. First, H_2 evolution is inhibited at all tested temperatures since the adsorption of $[Emim]^+$ cations and the formation of CO intermediate onto the electrode restrains proton adsorption and the competitive HER in the CO_2-saturated system.[40] The suppression of HER in the CO_2-saturated IL system can also be due to the formation of $[CO_2-Emim]^+$ complex on the Pt electrode interface, supported by the *in situ* spectroscopic evidence (sum frequency generation measurements).[41] This inhibition phenomenon can be further evidenced by the disappearance of the corresponding oxidation peaks between −0.9 and −2.0 V in the reverse anodic scan (see inset of Figure 3b). Second, the comparison of oxidation peak current densities at 0.2 to −1.0 V between CO_2- and N_2-saturated [Emim][NTf_2] gives rise to the relatively complex situation at different temperatures (Figure 4). For the sake of presentation, we will analyze the data in the three different temperature regions, including low temperature (−10 and −5 °C), 0 °C, and higher temperature (25 and 40 °C).

At −10 and −5 °C, the anodic peak current density $J_{pa'}$ (inset of Figure 3b) values in CO_2-saturated systems are much smaller than the J_{pa} (inset of Figure 3a) in N_2-saturated electrolytes (Figure 4). It is well-known that the viscosity of [Emim][NTf_2] at lower temperatures is greater than that at higher temperatures. Hence, the *in situ* formed imidazolium carbene is trapped in the electrode interface and difficult to diffuse to the outer bulk electrolyte. Imidazolium carbene has drawn significant attention due to its multifunctional application. On the one hand, the electrogenerated imidazolium carbene can serve as an active organic species to capture

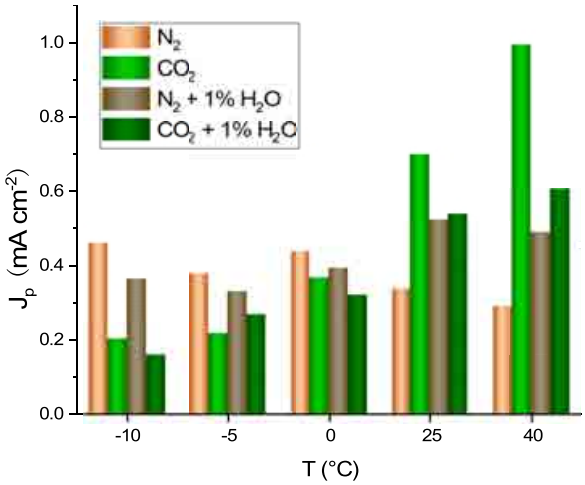

Figure 4. Histogram of J_p values in N_2- and CO_2-saturated [Emim][NTf_2] with and without 1% water at five different temperature points. J_p is the anodic peak current density between −0.09 and −0.76 V.

CO_2 and yield imidazolium carbene−CO_2 adduct ([$Emim^+-CO_2^-$]) through a coupling reaction between carbene and CO_2 as described in eq 4.[42−44] This reaction takes place in CO_2-

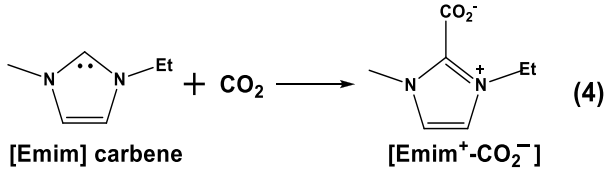

saturated [Bmim][BF_4] electrolysis cell on glassy carbon and several different metallic electrodes. In the comparison of the voltammograms with or without CO_2, due to the formation of imidazolium carbene−CO_2 adduct ([$Emim^+-CO_2^-$]), the oxidation current corresponding to the oxidation of imidazolium carbene back to the initial imidazolium cation is diminished because most of the imidazolium carbene has been used up by CO_2 coupling reaction.[39] Thus, the coupling product of [$Emim^+-CO_2^-$] is proposed as an electroinactive adduct, which may be thermally decomposed back to imidazolium carbene and CO_2.[45] On the other hand, the electron donation property of imidazolium carbene facilitates its strong adsorption on the metallic electrode surface for efficient CO_2 capture. Nakamura's study reveals that the

https://dx.doi.org/10.1021/acs.jpcc.0c06065
J. Phys. Chem. C 2020, 124, 26094−26105

electrochemical reaction between [Emim][BF_4] and the Cu electrode could produce a reduced imidazolium cation layer including imidazolium carbene, which could serve as the active site for CO_2 coupling.[7] On the basis of the above-mentioned prior works, it is suggested that the electrogenerated imidazolium carbene species are readily absorbed on the electrode interface at the lower temperatures in our system, which further captures the dissolved CO_2 to generate the electrochemically stable adduct [$Emim^+-CO_2^-$] according to eq 4. In this process, most of the electroactive imidazolium carbene is consumed by coupling with CO_2, so the oxidation peak current densities at about −0.5 V in CO_2-saturated electrolytes ($J_{pa'}$) is distinctly smaller than those in N_2 saturated ones (J_{pa}) (Figure 4). This result further supports that [$Emim^+-CO_2^-$] is an electroinactive adduct. Besides, although imidazolium-based IL can lower the energy necessary for intermediate formation in electrochemical CO_2 reduction, this activation of CO_2 to form a $CO_2^{\bullet-}$ radical requires an unusually high reduction potential of −1.9 V vs NHE.[13,46] What is more, the associated overpotential is not a constant and expectedly dependent on the electrode, medium, and temperature. For example, early studies have indicated that the Pt (111) electrode is less active[47] to reduce CO_2 to $CO_2^{\bullet-}$ radical in [Emim][NTf_2] with a cathodic potential even at −3.1 V at room temperature.[19] Therefore, it is plausible that −3.1 V is not negative enough for significant reduction of CO_2 to form $CO_2^{\bullet-}$ radicals following eq 1 on our polycrystalline Pt electrode at subzero temperature. As a consequence, the reactive imidazolium carbene formed at the electrode interface has to couple with CO_2 molecules to form the electroinactive adduct of [$Emim^+-CO_2^-$], which dominates the electrode process at a lower temperature.

At 0 °C, the $J_{pa'}$ in the CO_2 system is a little smaller than the J_{pa} in N_2 electrolyte, and the difference in the current density value (−69.94 μA cm^{-2}) is much smaller than those at the lower temperatures at −10 and −5 °C (Figure 4). It is well accepted that the viscosity of [Emim][NTf_2] at 0 °C is less than those at −10 and −5 °C, and thus a portion of the imidazolium carbene can diffuse away from the Pt electrode interface. Moreover, the increased temperature from −10 and −5 to 0 °C can enhance the electrochemical activity toward CO_2 reduction. Thus, a potential of −3.1 V at 0 °C is enough to electrochemically reduce the adsorbed CO_2 to generate $CO_2^{\bullet-}$ radicals. More importantly, compared to imidazolium carbene, [$Emim^{\bullet}$] radicals are more easily formed by reducing imidazolium cation at less negative potential following eq 2. As a result, a radical−radical coupling reaction between $CO_2^{\bullet-}$ and [$Emim^{\bullet}$] can take place to form a new adduct of [EmimH−CO_2^-] in a reduction pathway according to eqs 1, 2, and 5. In contrast, the new adduct of [EmimH−CO_2^-] is

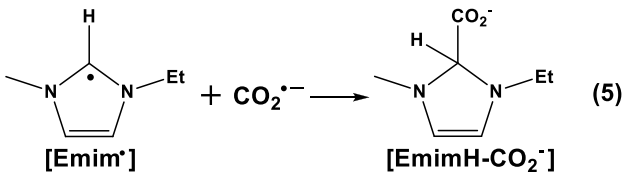

electroactive and may be readily oxidized back to the initial imidazolium cation. It is the oxidation reaction of [EmimH−CO_2^-] that makes the $J_{pa'}$ value in the CO_2 system is much bigger than those at −10 and −5 °C (Figure 3a). Nevertheless, the $J_{pa'}$ value is slightly smaller than the J_{pa} observed in the N_2 system, which provides a strong indication that a fraction of the cathodically generated imidazolium carbene was coupled with CO_2 to form the electroinactive [$Emim^+-CO_2^-$] adduct. Hence, we can speculate that competitive reaction pathways of eqs 4 and 5 on the electrode interface exist at 0 °C.

At 25 and 40 °C, inversely, the $J_{pa'}$ values in CO_2-saturated systems are much bigger than the J_{pa} in N_2-saturated electrolytes. At these high temperatures, the aforementioned −3.1 V can offer enough activation energy for the significant reduction of CO_2 to form $CO_2^{\bullet-}$ radicals, which will spontaneously couple to an abundant amount of [$Emim^{\bullet}$] radicals for the production of the electroactive [EmimH−CO_2^-] on the electrode interface. Additionally, at these higher temperatures, [Emim][NTf_2] has a smaller viscosity than that at 0, −10, and −5 °C. Compared to those at 0, −10, and −5 °C, the surface species formed at 25 and 40 °C are easier to diffuse away from the electrode interface. The imidazolium cations and CO_2 molecules can thus continuously diffuse toward the Pt electrode interface from the bulk electrolyte and are electrochemically reduced to [$Emim^{\bullet}$] and $CO_2^{\bullet-}$ radicals to replenish the consumed portion. A small amount of the [$Emim^{\bullet}$] radicals can probably be further reduced to imidazolium carbene species, but the carbene species will rapidly diffuse away from the electrode interface at these higher temperatures. This is verified by the decreased oxidation peak current density J_{pa} in the N_2-saturated electrolyte at the higher temperatures of 25 and 40 °C (Figure 4) since the J_{pa} values are solely responsible for the oxidation of the cathodically generated imidazolium carbene species. [EmimH−CO_2^-] is electroactive and can easily be oxidized back to the initial imidazolium cation, hence displaying much larger oxidation peak currents than those in the N_2-saturated system. Therefore, at the higher temperatures, the electrode reaction pathway in CO_2-saturated system is dominated by the coupling reaction between [$Emim^{\bullet}$] and $CO_2^{\bullet-}$ radicals to form [EmimH−CO_2^-] adduct as shown in eq 5.

2. Comparison of CO_2 Reduction in [Emim][NTf_2] vs [Bmpy][NTf_2] at Varying Temperature. To further verify our findings regarding temperature control for CO_2 reduction in imidazolium IL, we performed identical experiments in a control IL (i.e., [Bmpy][NTf_2]) with the same anion but a much more stable and bulky [$Bmpy^+$] cation. In contrast to [$Emim^+$] cations which are more reactive and play a key catalytic role in electrochemical CO_2 reduction by the formation of radicals,[7,25] [$Bmpy^+$] cation has the effect of modifying the electrochemical double-layer.[21] With the characterization of the core catalytic effect of [$Emim^+$] cations in hand, we examined the electrochemical reduction of CO_2 in [Emim][NTf_2] at different temperatures and compared to those in [Bmpy][NTf_2] electrolyte. As illustrated in Figure S3, all CV features in [Emim][NTf_2] at different temperatures present the much more distinct cathodic behaviors than those in [Bmpy][NTf_2]. It can be evidenced by the significantly earlier onset potentials (about from −1.1 to −2.1 V) and much bigger reduction current densities at −3.1 V (about 4.85 to 10.67 mA cm^{-2}) in [Emim][NTf_2] than the corresponding values in [Bmpy][NTf_2] (E_0: about from −2.0 to −2.3 V; J @ −3.1 V: about from 0.63 to 1.53 mA cm^{-2}) (Figure 5). These results confirm that imidazolium cation is more active and easily reduced to the reduced imidazolium species to facilitate CO_2 reduction compared to that of the inert [$Bmpy^+$] cation. Moreover, all CV curves in [Emim][NTf_2] present stronger anodic peak responses (at about from −0.15 to −0.9 V)

https://dx.doi.org/10.1021/acs.jpcc.0c06065
J. Phys. Chem. C 2020, 124, 26094−26105

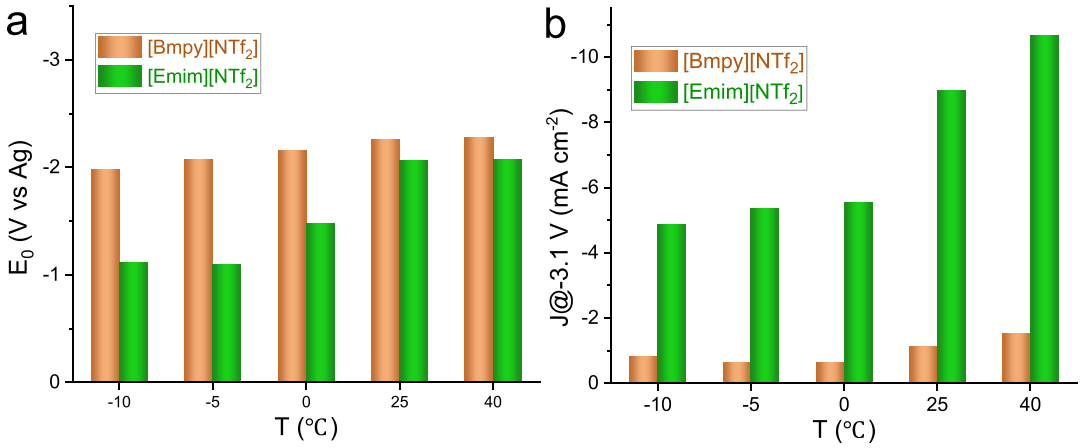

Figure 5. Comparative histograms of onset potentials (a) and currents at −3.1 V (vs Ag) (b) in CO_2-saturated [Emim][NTf_2] and [Bmpy][NTf_2] systems at different temperatures.

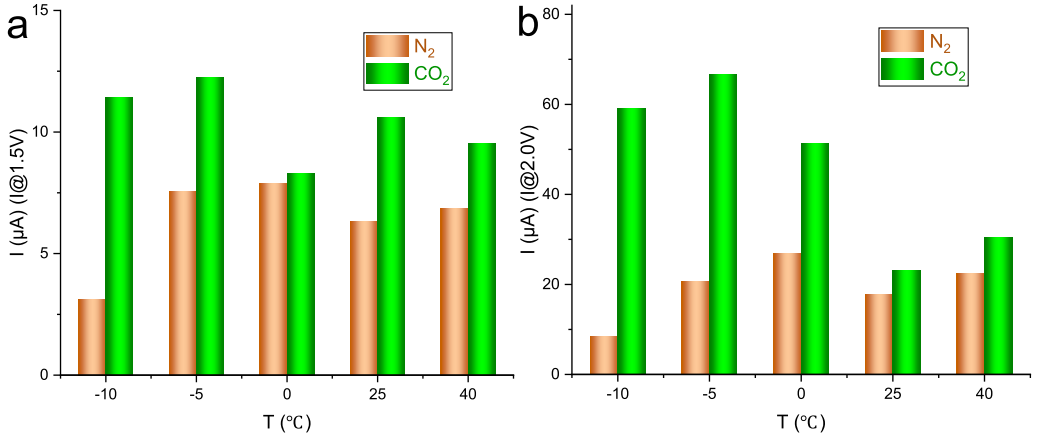

Figure 6. Histograms of currents at (a) 1.5 and (b) 2.0 V (vs Ag) in N_2- and CO_2-saturated [Emim][NTf_2] at different temperatures during positive scanning from 0 to 2.0 V (vs Ag).

resulting from the oxidation of the reduced imidazolium species and their adduct with CO_2. In contrast, the CV curves in [Bmpy][NTf_2] only demonstrate relatively weak anodic electrochemical behaviors (Figure S3). Even though the trend of the changes of E_0 and current at −3.1 V are similar, the magnitude of change upon temperature is much bigger in [Emim][NTf_2] compared to in [Bmpy][NTf_2] IL. The above data further establish that the $[Emim]^+$ cation is the more active species for electrochemical reduction of CO_2 compared to $[Bmpy]^+$.

As shown in Figure S4 (Supporting Information) and Figure 6, we further studied the CO formation as a CO_2 reduction product at the Pt electrode by first performing a cathodic scan between 0 and −2.0 V to reduce CO_2. Then, we immediately performed an anodic scan between 0 and 2.0 V to oxidize CO. Our early work shows that both CO and anion $[NTF_2]^-$ can be electrochemically oxidized on Pt electrode at the potential of 1.5 V in an inert nitrogen environment. Figure 6 compares the oxidation currents at 1.5 and 2.0 V in N_2- and CO_2-saturated [Emim][NTf_2]. It is clearly shown that the oxidation currents in CO_2-saturated IL are bigger than those in N_2-saturated IL system at both 1.5 and 2.0 V. This indicates that CO was formed during the CO_2 reduction process and that the CO was subsequently oxidized during the anodic scan from 0 to 2.0 V. Notably, at both 1.5 and 2.0 V, the amounts of increased currents at low temperatures of −10 and −5 °C are obviously bigger than those at high temperatures of 0, 25, and 40 °C. This result can be explained that the IL−electrode interface structure packed more densely at low temperatures facilitating the CO_2 dissolution and adsorption providing higher CO_2 reduction current. Our early work shows that this double potential experiment can minimize CO poisoning of the Pt electrode.[48] In order to estimate the contributions of [Emim][NTf_2] toward the observed enhancement in the catalytic activity of the CO_2 reduction reaction, we also compared the charges of these CO anodic stripping experiments at different temperatures (for procedure, see Supporting Information and Figure S4). As illustrated in Figure S4f, the charges in [Emim][NTf_2] are much bigger than those in [Bmpy][NTf_2] at corresponding temperature points. The larger charge values in [Emim][NTf_2] can result from the formation of reduced imidazolium species at a molecular level on the electrode surface that catalyzes CO_2 reduction. Another interesting find extracted from the CVs of CO stripping voltammetry (Figure S4) is the distinct negative-shift in peak potentials and the enhanced anodic currents of the CO oxidation process in [Emim][NTf_2] compared to [Bmpy]-[NTf_2]. This result highly supports more efficient catalytic activity for electrochemical CO_2 reduction in [Emim][NTf_2] than that in [Bmpy][NTf_2].

Tafel plots have been widely used to evaluate kinetic parameters of redox reactions, especially for irreversible or

https://dx.doi.org/10.1021/acs.jpcc.0c06065
J. Phys. Chem. C 2020, 124, 26094−26105

quasi-reversible systems. Hence, the kinetics of CO_2 reduction in both [Emim][NTf_2] and control [Bmpy][NTf_2] systems is assessed by analyzing their Tafel curves (Figure S5). The two groups of Tafel data (Table S3) establish that [Emim][NTf_2] follows the many mechanistic pathways different from [Bmpy][NTf_2] for electrochemical CO_2 reduction. [Bmpy]-[NTf_2] gives rise to a Tafel slope range from 97 to 126 mV dec^{-1} at different temperatures, which is close to the 118 mV dec^{-1} indexing a rate-determining one-electron transfer for the formation of $CO_2^{\bullet-}$ from the adsorbed CO_2.[49,50] By contrast, the slopes in [Emim][NTf_2] are observed in the range of 47 to 82 mV dec^{-1}. These are much closer to 59 mV dec^{-1}, supporting the mechanism that the reduced [Emim] layer on the electrode occurs before a single-electron transfer to form $CO_2^{\bullet-}$ prior to a rate-limiting chemical step.[51] It is thus inferred that the imidazolium carbene species formed provides a more electron-rich electrode surface owing to the strong σ-donation, which in turn can accelerate CO_2 activation by stabilizing the $CO_2^{\bullet-}$ intermediate more effectively before the rate-limiting reaction.[4]

3. Temperature Effects on the IL-Electrode Double-Layer Structure. Since electrochemical CO_2 reduction in an IL electrolyte occurs in a very thin electrical double-layer region and involves complex chemical components,[52] the chemical composition in the electrochemical double-layer is expectably important for the CO_2 reduction reaction. The double-layer capacitance (C) of an IL−electrode interface can be expressed by[53]

$$C = \frac{\epsilon\epsilon_0}{d} \tag{6}$$

where ϵ is the dielectric constant of the material between the plates, ϵ_0 is the permittivity of free space, and d is the distance between the plates.[54] Thus, the double-layer capacitance is inversely proportional to the thickness of the electric double-layer. Also, both experimental and theoretical observations have demonstrated that the double-layer capacitance in IL is temperature-dependent.[54,55] As a consequence, it is imperative and significant to analyze temperature effects on the IL−electrode double-layer structure. The double-layer charging current is directly related to the double-layer capacitance, and so it can provide the temperature effects on the IL-electrode double layer. Figure S6a and Figure S6b summarize the double layer charging current measured at double layer region (where there are no faradaic processes, at about 0.836 V in [Emim][NTf_2] and −0.036 V in [Bmpy][NTf_2]) vs temperature in both ILs saturated with N_2 or CO_2, respectively. As shown in Figure S6c, in [Emim][NTf_2] saturated with CO_2, the double layer charging current changes little with the temperature change. In contrast, when [Emim][NTf_2] is saturated with N_2, the double layer charging current decreases with increasing temperature. Interestingly, in [Bmpy][NTf_2] saturated with CO_2 or N_2, the double layer charging current has a maximum at −5 °C with a positive slope from −10 to −5 °C but a negative slope from −5 to 25 °C. More impressively, all capacitance values at different temperatures in [Bmpy]-[NTf_2] are visibly smaller than those in [Emim][NTf_2]. The above results indicate that the small-sized reactive $[Emim]^+$ cation can be more easily adsorbed on the electrode interface to form the more organized and thinner double-layer compared to $[Bmpy]^+$ cation. Besides, the inert and bulky $[Bmpy]^+$ cations are unable to entrap CO_2 molecules and form stable double-layer in [Bmpy][NTf_2] electrolyte, thus exhibiting variable capacitance concerning temperature such as under N_2 atmosphere. A computational study by Boda et al.[54,56,57] shows that the capacitance is both density- and temperature-dependent. In accordance with the predictions based on the density, the capacitance increases nearly linearly with the increasing density. Since the density of ILs increases with the decrease in temperature, the capacitance should decrease with an increase in temperature. In N_2-saturated [Emim][NTf_2], the double layer charging current decreases with an increase in temperature, showing a predominant density effect. In the CO_2-saturated [Emim][NTf_2], there are small changes of double layer charging current vs temperature due to two opposite effects of temperature on the double-layer capacitance. At high temperatures, the thickness of the double layer can increase because of the increased thermal energy. This leads to a decreased capacitance with increasing temperature. On the other hand, at low temperatures and low electrode charge, the ion−ion interactions become strong compared to the ion−electrode interaction, and the counterions tend to pull away from the electrode causing a thicker electrical double layer and a decreased capacitance with decreasing temperature. At a higher electrode charge, the ion−electrode interaction becomes dominant and the capacitance will increase with the temperature. In our case, at a higher electrode charge, the $[Emim]^+$−Pt electrode interaction becomes dominant. Both density and ionic association effects could lead to small dependence of capacitance with the temperature in [Emim]-[NTf_2] saturated with CO_2. Since [Bmpy][NTf_2] is bulky and has smaller interaction with the Pt electrode compared to [Emim][NTf_2], the capacitance has a negative slope at a high temperature and a positive slope at a low temperature in the [Bmpy][NTf_2] saturated with N_2 or CO_2. Both [Emim][NTf_2] and [Bmpy][NTf_2] results are consistent with those predicted by Boda's series reports taking into the effects of temperature-dependent density and ionic association for the anomalous temperature dependence of the capacitance of the electrical double layer.

4. Effects of Water on CO_2 Reduction Mechanisms in [Emim][NTf_2]. To investigate the water effect on CO_2 reduction mechanisms, we carried out CV experiments in the [Emim][NTf_2] with added 1% of the water that was well mixed with the IL. Since [Emim][NTf_2] is hydrophobic, the added water is not forming a homogeneous solution with [Emim][NTf_2] and the water is likely dispersed at the IL−Pt interface.[58] We used the same experimental conditions as those pristine IL systems to study the effects of water on CO_2 reduction mechanisms at a celsius above and below zero temperature.

We compared the CVs in N_2 and CO_2 with and without 1% adding water in [Emim][NTf_2] IL at five temperatures, and typical CVs at −10, 0, and 40 °C were presented in Figure S8a−c. As shown in Figures 4 and S8, at 40 °C, in the N_2-saturated [Emim][NTf_2], the addition of 1% H_2O almost did not change the cathodic onset potential (HER and reduction of [Emim]) at about −1.92 V but leads to the slight increase in the oxidation peak current at around −1.69 V (H_2 oxidation) and −0.69 V (oxidation of the reduced [Emim] species). In the CO_2-saturated [Emim][NTf_2], the addition of 1% H_2O almost did not change the cathodic onset potential (reduction of CO_2 and [Emim]) at about −2.03 V but leads to the distinct *decrease* in the oxidation peak current at the almost unchanged peak potential of around −0.88 V (oxidation of the reduced [Emim] species and the reduced CO_2 species). The reduction

https://dx.doi.org/10.1021/acs.jpcc.0c06065
J. Phys. Chem. C 2020, 124, 26094−26105

current in the IL containing water is almost the same as that in the pure IL system in most of the potential window.

Molecular dynamics (MD) and the experimental study suggest that water in hydrophilic [Bmim][BF_4] is adsorbed less on the electrode surface than in hydrophobic IL at negative electrode polarization.[59,60] [Emim][NTf_2] is hydrophobic. Feng et al.'s MD results of hydrophobic ILs ([Bmim][PF_6] and [Bmim][NTf_2]) are closer to our [Emim][NTf_2] system. Their results show that water molecules tend to accumulate within subnanometer distance from charged electrodes and the preferential positions of water molecules in double layers are determined by the balance of the tendency to follow the positions of the maximal absolute value of the electrical field, the association with their ionic surroundings, and the propensity to settle at positions where more free space is available.[61] We rationalize that the majority of water molecules are expected to be at the Pt electrode and IL interface at negative electrode potential for the reduction processes. ATR-IR studies of the molecular state of water in ILs with $[Bmim]^+$ cations and different anions including $[NTf_2]^-$ anions show that water is present mostly in the "free" (not self-associated) state when the concentrations of dissolved water are in the range 0.2−1.0 mol dm^{-3}.[58] This study also shows that most of the water molecules at these concentrations exist in H-bonded complexes: anion···HOH···anion. It is expected that for the cathodic process, the adsorption of water at the Pt surface should reduce the amount of CO_2 adsorption and the adsorption of $[Emim]^+$ cation. As a result, CV in cathodic potentials should show higher HER current, lower CO_2 reduction current, and smaller $[Emim]^+$ reduction current, and these combined processes are likely the reason little change in cathodic currents with or without water is observed. For the anodic process, the decrease of CO_2 reduction and $[Emim]^+$ reduction processes due to lesser amounts of CO_2 and $[Emim]^+$ in the presence of a higher amount of water led to a decrease of anodic current observed.

At 0 °C, in the N_2-saturated [Emim][NTf_2], the addition of 1% H_2O leads to a visibly *negative* shift of cathodic onset potential (HER and reduction of [Emim]) from −1.45 to −1.67 V and an almost equal oxidation peak current at nearly same potentials of around −1.25 V (H_2 oxidation) and −0.25 V (oxidation of the reduced [Emim] species) compared to those pristine [Emim][NTf_2]. The reduction current in the IL containing water is almost the same as that in the pristine IL system in most of the potential window. In the CO_2-saturated [Emim][NTf_2], the addition of 1% H_2O results in an obviously *positive* shift of the cathodic onset potential (reduction of CO_2 and [Emim]) from −1.48 to −1.36 V and a slightly reduced oxidation peak current with almost unchanged peak potential at about −0.44 V (oxidation of the reduced [Emim] species and the reduced CO_2 species). From the onset potential to the negative direction, the reduction current in the IL containing water is distinctly larger than that in the pristine IL system.

At zero temperature, bulk water will freeze. However, the water molecules in our system are likely confined between the high density of IL [Emim][NTf_2] and the Pt electrode surface. Molecular dynamics simulations show that on cooling, the confined water, which has an imperfect random hydrogen-bonded network, transforms into a bilayer amorphous phase with a perfect network (owing to the formation of various hydrogen-bonded polygons) but no long-range order.[62] These more ordered water molecules require higher energy for the HER and $[Emim]^+$ reduction leading to the negative shift of the cathodic onset potentials. Additionally, there is a strong correlation between the ratio of unoccupied space in pure ILs and their ability to absorb CO_2.[63] Thus, we rationalize that the increasing of the packing of the ILs at zero temperature would make these water molecules likely in close proximity with the adsorbed CO_2 molecules in the unoccupied space in the IL. This would facilitate CO_2 reduction processes and cause a positive shift in cathodic onset potentials.

At subzero temperature (−10 °C) in the N_2-saturated [Emim][NTf_2], the addition of 1% H_2O leads to a significant *positive* shift in cathodic onset potential (HER and reduction of [Emim]) from −1.26 to −1.58 V and a distinctly decreased oxidation peak current at around −0.98 V (H_2 oxidation) and −0.06 V (oxidation of the reduced [Emim] species). From the onset potential to the negative direction, the reduction current in the IL containing water in N_2 is much larger than that in the pristine IL system. In the CO_2-saturated [Emim][NTf_2], the addition of 1% H_2O results in a significant *negative* shift in cathodic onset potential (reduction of CO_2 and [Emim]) from −1.11 to −1.60 V and the oxidation peak potential from around −0.20 to −0.64 V (oxidation of the reduced [Emim] species and the reduced CO_2 species). From the onset potential to the negative direction, the reduction current in the IL containing water is much smaller than that in the pristine IL system. At subzero temperatures, water is expected to form solid ice at the interface, weakening the anion···HOH···anion complex that would facilitate HER to occur at a more positive potential. Furthermore, the density of IL increases with a decrease in temperature, making the unoccupied space in the ILs less than those at higher temperatures. This would explain the negative shift of CO_2 reduction potential and smaller CO_2 reduction currents.

We interpret our results based on the density and temperature effects. The density changes with temperature will include the effects of lower entropy. Cleary the lower the temperature, the higher is the density and the lower is the entropy at the IL−electrode interface. Nevertheless, we expect to observe greater entropic effects of water molecules in [Emim][NTf_2] than in [Bmpy][NTf_2]. Without the prescence of CO_2 redox process, the entropy of the IL−electrode interface should be low at electrified [Emim][NTf_2]−Pt electrode interface since it is more ordered due to $Emim^+$−electrode interaction when compared to that of the [Bmpy]-[NTf_2]−Pt interface. Due to the different amounts of water molecules in hydrophobic vs hydrophilic IL, the overall state of [Emim][NTf_2] and [Bmpy][NTf_2]−Pt electrode interface double layers should be more separate and have less opportunity to have substantial entropy increases from mixing when compared to small and hydrophilic ions.[64]

5. DFT Calculations and Summary of Temperature Effects on CO_2 Reduction Mechanisms in [Emim][NTf_2].

Our experimental results show that CO_2 reduction in an imidazolium IL could proceed via five different reaction pathways due to the parallel reduction of the cation imidazolium and the coupling reactions between the products of $CO_2^{\bullet-}$ and imidazolium radicals. Varying the temperature allows the tuning of the viscosity and IL−electrode interface structure that affects CO_2 reaction pathways. DFT calculations were performed to estimate the free energy changes and validate our findings regarding reactions 1−5. B3LYP functional and the 6-31++G** basis set were used and modeled by the IEF-PCM formalism with ε = 11.7 [65] of [Emim][NTf_2]. The full results are given in the Supporting Information, and a

https://dx.doi.org/10.1021/acs.jpcc.0c06065
J. Phys. Chem. C 2020, 124, 26094−26105

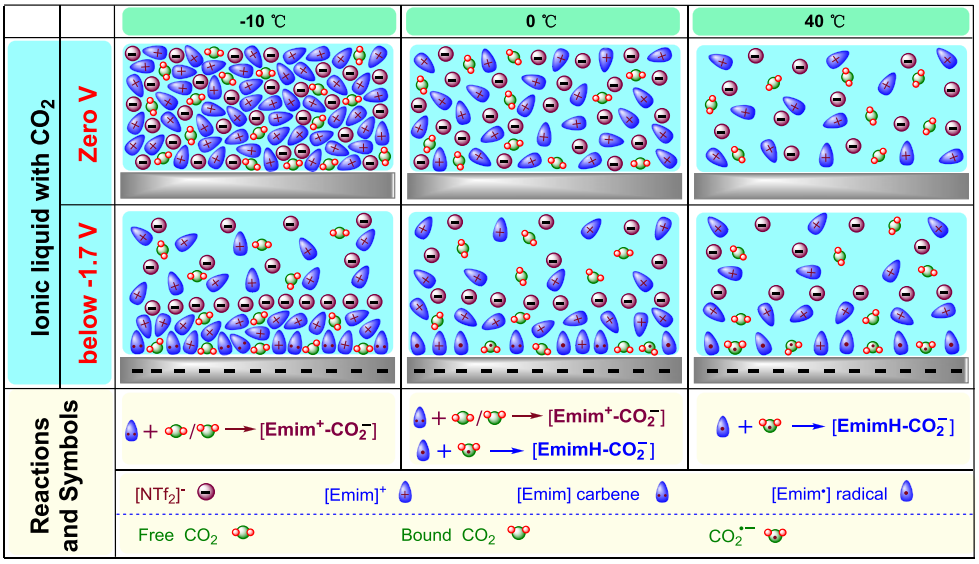

Figure 7. Schematic of prospective IL/Pt interface process under 0 V and catalytic pathways for electrochemical reduction of CO_2 under below −1.7 V (this potential should be ensured according to the onset potential CO_2 starting to be reduced) at different temperatures. Note that free CO_2 molecules are in a linear structure. The bound CO_2 molecules or their derived species have a bent structure.

summary is given in Figures S9−S11 and Tables S4−S7. All the reactions show substantial negative free energy and are thermodynamically favorable.

Reaction 1 is the reduction of CO_2 to form $CO_2^{\bullet-}$. It has a free energy of −235.2 kJ/mol and corresponds to a reduction potential of −2.00 V vs NHE (taking the absolute hydrogen electrode potential of 4.44 V). This value compares well with the experimental value of −2.1 V. Reaction 2 is the reduction of the IL imidazole cation ($[Emim]^+$) to form [Emim•] and also has a very favorable free energy of −215.6 kJ/mol. Hence, both reductions are quite feasible in the IL environment. Reaction 3 is the reduction of the imidazole cation to form carbene and H_{ads} on the platinum electrodes. DFT calculations for the imidazole cation and the carbene are straightforward. The estimation of the free energy of H_{ads} required the straightforward DFT calculation of the gas phase H atom free energy (0.50100 AU) and the addition of the reported free energy for H atom adsorption on Pt(111) surface (0.45 eV/H atom)[66] summing to 0.51754 AU. This allows a reasonable estimate of the overall energy of reaction 3 giving ΔG = −109.7 kJ/mol. Thus, reaction 3 is predicted to be favorable but less so than reactions 1 and 2.

Reaction 4 is a direct reaction of the carbene with the neutral CO_2 molecule. The free energy of −47.7 kJ/mol is modestly favorable in part owing to a negative entropy change ΔS = −103.8 J/(mol K). Nevertheless, the reaction is predicted to go at room temperature and would be more favored at lower temperatures due to negative entropy. The adsorption of carbene on Pt electrode will compete with reaction 4, and this is not taken into account in the calculation. Another competitive reaction, reaction 5, is the coupling of imidazole radical with CO_2 anion radical. This has a significantly larger free energy ΔG = −138.9 kJ/mol and even with its more negative entropy change (ΔS = −190.4 J/(mol K)). This path is predicted to be favored at 40 °C. For example, since reaction 5 has a ΔG = −138.9 kJ/mol at 25 °C and reaction 4 at 25 °C has a ΔG = −47.7 kJ/mol, reaction 5 is predicted to be favored at 25 °C, as found experimentally. However, favoring of reaction 4 at low temperatures is not predicted since reaction 5 is more exergonic at all experimental temperatures. This suggests other factors are at play such as temperature-dependent surface absorption of carbene as well as double-layer structure. The higher the temperature, the lesser is the formation of ion-pair due to the weakening of Coulombic interactions between cation and anions. Subsequently, more ions are available for adsorption at the Pt electrode interface with increasing temperature. Increasing temperature can also weaken the hydrogen bonding between the anion and hydrogen from the imidazolium ring.[53] Our rationalization is supported by the analysis of IL double capacitance results.

We also calculated the electrode potentials for reactions 2 and 3 and the temperature effects on the free energy change for reactions 4 and 5. The predicted free energy change for reaction 4 in which CO_2 adds to the carbene is more favorable at lower temperatures. However, as the temperature increases, dissociation of the complex would be expected as the free energy drops to only −46 kJ/mol at 40 °C. For reaction 5, the free energy of the reaction is far more favorable and the temperature should not be a factor in the dissociation of the complex once formed as even at 40 °C the free energy change for the reaction is −137 kJ/mol. The formation of the carbene at low temperatures is therefore in agreement with the DFT calculations as is its loss at higher temperatures.

The above experimental and DFT results suggest temperature plays a significant role in controlling the CO_2 reduction reaction pathways in $[Emim][NTf_2]$ IL. The viscosity of IL is temperature-dependent, and thus the viscosity of the IL will be modified by temperature. Additionally, ions with permanent dipole moments interact with each other via directional electrostatic interactions as well as van der Waals interactions and hydrogen bonding. These weak to moderate interactions cause the orientations of ions to be strongly temperature-dependent. At high temperatures, the various forces that maintain the IL structure at low temperatures are overcome and other orientations in the IL become more populated. Together, the change of viscosity and interaction forces due to temperature change will result in the change of the IL−

https://dx.doi.org/10.1021/acs.jpcc.0c06065
J. Phys. Chem. C 2020, 124, 26094−26105

electrode double layer properties, which renders the control of the reaction pathways for CO_2 reduction reactions via temperature effects on (i) the IL−Pt electrode interface structure and properties, (ii) the mass transport of the reactant and intermediates, and (iii) the adsorption and solubility of the intermediates species. The catalytic mechanism of [Emim]-[NTf_2] to CO_2 at different temperatures can be summarized as follows. The higher the temperature, the more $CO_2^{\bullet-}$ is formed. At subzero temperatures, due to lack of $CO_2^{\bullet-}$ radicals, the coupling reaction between the formed imidazolium carbene and CO_2 governs the electrode process, which results in the formation of imidazolium carboxylate ([$Emim^+$−CO_2^-]) and the deactivation of the $[Emim]^+$ cation as a cocatalyst. At near 0 °C, the availability of a limited amount of $CO_2^{\bullet-}$ radicals enables a radical−radical coupling reaction between these $CO_2^{\bullet-}$ and some of [$Emim^{\bullet}$] radicals before [$Emim^{\bullet}$] radicals were reduced to carbene. Meanwhile, some other [$Emim^{\bullet}$] radicals can be further reduced to [Emim] carbene, which consequently couples with CO_2 to form the adduct of [$Emim^+$−CO_2^-]. At higher temperature (25 and 40 °C), a substantial amount of $CO_2^{\bullet-}$ can be formed and can couple to almost all formed [$Emim^{\bullet}$] radicals through a radical−radical coupling reaction, which is the predominant electrode reaction, and the pathway of reduction of [$Emim^{\bullet}$] radicals to carbene is inhibited. Therefore, the mechanism and pathway of electrocatalytic CO_2 in [Emim][NTf_2] are highly temperature-dependent. Figure 7 summarizes the interfacial structures of the IL−electrode interface at initial potential zero volt and at the onset potential (−1.7 V) where the CO_2 reduction processes start at three representative temperatures (−10, 0, and 40 °C) in our experiments without considering the effect of trace water. At zero volt, which is near the point of zero charges of Pt, the electrical polarization effect is negligible. At increased negative electrical potential (−1.7 V), the strength of electrostatic interionic interaction increases with a decreasing temperature that leads to the formation of ionic pairs and even more complex ionic aggregates. The IL−electrode interface is a mixture of free ions, ion pairs, and CO_2.

CONCLUSIONS

Temperature is considered an important factor in deciding electrochemical reaction kinetics. However, the study of the electrode reactions at subzero temperature has rarely been carried out since traditional aqueous and some nonaqueous electrolytes freeze at low temperatures. The unique physicochemical properties of ILs provide an excellent solvent and electrolyte system to study interface electrochemistry in the ILs for electrocatalysis and chemical sensors at extreme temperatures and harsh environmental conditions. The motivation to convert CO_2, a potent greenhouse gas, to useful chemicals has driven significant research toward the study of the electrochemical reduction of CO_2 in IL electrolytes. A series of recent literature reports show that the imidazolium cation can catalyze the reduction of CO_2 via different pathways and the ion-dependent reaction pathways of CO_2 electroreduction were previously linked to the electrical double-layer effects. In this work, we systematically studied CO_2 reduction in [Emim][NTf_2] at varying temperatures (−10 to 40 °C) on Pt electrode by CV and anodic stripping voltammetry. We also compared it to that of CO_2 reduction in [Bmpy][NTf_2], which has a much more inert and bulky $[Bmpy]^+$ cation. Our results show that CO_2 reduction pathways can be controlled by temperature. At temperatures below zero, the CO_2 reduction to form $CO_2^{\bullet-}$ radicals is limited, and the imidazolium cation reduction and its coupling reaction are dominant that result in the formation of electroinactive imidazolium carboxylate ([$Emim^+$−CO_2^-]). At 0 °C, there are two competitive reaction pathways: the coupling reaction of the formed imidazolium carbene with CO_2 and the coupling reaction of [$Emim^{\bullet}$] radicals with $CO_2^{\bullet-}$ radicals. At higher temperatures (25 and 40 °C), CO_2 is reduced to $CO_2^{\bullet-}$, which subsequently couples with [$Emim^{\bullet}$] radicals. This reaction inhibits the reduction of [$Emim^{\bullet}$] radicals to carbene. Since the viscosity and the weak to moderate molecular forces of different interactions (ion−ion, van der Waals, hydrogen bonding, ion−dipole, and dipole−dipole) depend on temperature, the resulting properties of ILs depend on which interactions are prevalent at a certain temperature. At the interface, the structure of the electric double-layer can be affected by the electric field, those weak to moderate molecular interactions among ILs and the redox intermediates, and their interactions with the electrode material. Our study demonstrates that using temperature can control the CO_2 reduction pathways in imidazolium-based IL by tuning the viscosity and those temperature-dependent forces via their cumulative effects on the mass transport and solubility of reactant and intermediates and the electric double layer structures and properties.

ASSOCIATED CONTENT

Supporting Information

The Supporting Information is available free of charge at https://pubs.acs.org/doi/10.1021/acs.jpcc.0c06065.

Figures S1−11 and Tables S1−S7 showing the schematic diagram and optical photograph of the electrochemical cell, CV curves, Tafel plots, anodic current densities at capacitance potential, and DFT calculation data (PDF)

AUTHOR INFORMATION

Corresponding Author

Xiangqun Zeng − *Department of Chemistry, Oakland University, Rochester, Michigan 48308, United States;* orcid.org/0000-0003-3867-226X; Email: zeng@oakland.edu

Authors

Tianrong Zhan − *Department of Chemistry, Oakland University, Rochester, Michigan 48308, United States; Key Laboratory of Optic-Electric Sensing and Analytical Chemistry for Life Science (Ministry of Education), Qingdao University of Science and Technology, Qingdao, Shandong 266042, China;* orcid.org/0000-0001-8728-2829

Anil Kumar − *Department of Chemistry, Oakland University, Rochester, Michigan 48308, United States;* orcid.org/0000-0002-9979-7798

Michael Sevilla − *Department of Chemistry, Oakland University, Rochester, Michigan 48308, United States;* orcid.org/0000-0001-8799-5458

Arun Sridhar − *Department of Chemistry, Oakland University, Rochester, Michigan 48308, United States*

Complete contact information is available at: https://pubs.acs.org/10.1021/acs.jpcc.0c06065

Notes

The authors declare no competing financial interest.

https://dx.doi.org/10.1021/acs.jpcc.0c06065
J. Phys. Chem. C 2020, 124, 26094−26105

■ ACKNOWLEDGMENTS

This material is based upon work supported by the National Science Foundation (NSF) award 1913640.

■ REFERENCES

(1) Qiao, J.; Liu, Y.; Hong, F.; Zhang, J. A review of catalysts for the electroreduction of carbon dioxide to produce low-carbon fuels. *Chem. Soc. Rev.* **2014**, *43*, 631−675.
(2) Francke, R.; Schille, B.; Roemelt, M. Homogeneously catalyzed electroreduction of carbon dioxide-methods, mechanisms, and catalysts. *Chem. Rev.* **2018**, *118*, 4631−4701.
(3) Schwarz, H. A.; Dodson, R. W. Reduction potentials of CO_2- and the alcohol radicals. *J. Phys. Chem.* **1989**, *93*, 409−414.
(4) Sun, Z.; Ma, T.; Tao, H.; Fan, Q.; Han, B. Fundamentals and challenges of electrochemical CO_2 reduction using two-dimensional materials. *Chem.* **2017**, *3*, 560−587.
(5) Lau, G. P.; Schreier, M.; Vasilyev, D.; Scopelliti, R.; Gratzel, M.; Dyson, P. J. New insights into the role of imidazolium-based promoters for the electroreduction of CO_2 on a silver electrode. *J. Am. Chem. Soc.* **2016**, *138*, 7820−7823.
(6) Faggion, D.; Goncalves, W. D. G.; Dupont, J. CO_2 electroreduction in Ionic liquids. *Front. Chem.* **2019**, *7*, 1−8.
(7) Wang, Y.; Hayashi, T.; He, D.; Li, Y.; Jin, F.; Nakamura, R. A reduced imidazolium cation layer serves as the active site for electrochemical carbon dioxide reduction. *Appl. Catal., B* **2020**, *264*, 118495.
(8) Agarwal, J.; Shaw, T. W.; Stanton, C. J.; Majetich, G.; Bocarsly, A. B.; Schaefer, H. F. NHC-containing manganese(I) electrocatalysts for the two-electron reduction of CO_2. *Angew. Chem., Int. Ed.* **2014**, *53*, 5152−5155.
(9) Niu, D.; Wang, H.; Li, H.; Wu, Z.; Zhang, X. Roles of ion pairing on electroreduction of carbon dioxide based on imidazolium-based salts. *Electrochim. Acta* **2015**, *158*, 138−142.
(10) Ahrenberg, M.; Beck, M.; Neise, C.; Keßler, O.; Kragl, U.; Verevkin, S. P.; Schick, C. Vapor pressure of ionic liquids at low temperatures from AC-chip-calorimetry. *Phys. Chem. Chem. Phys.* **2016**, *18*, 21381−21390.
(11) Zhan, T.; Tan, Z.; Tian, X.; Hou, W. Lonic liquid functionalized graphene oxide-Au nanoparticles assembly for fabrication of electrochemical 2,4-dichlorophenol sensor. *Sens. Actuators, B* **2017**, *246*, 638−646.
(12) Cadena, C.; Anthony, J. L.; Shah, J. K.; Morrow, T. I.; Brennecke, J. F.; Maginn, E. J. Why is CO_2 so soluble in imidazolium-based ionic liquids ? *J. Am. Chem. Soc.* **2004**, *126*, 5300−5308.
(13) Sun, L.; Ramesha, G. K.; Kamat, P. V.; Brennecke, J. F. Switching the reaction course of electrochemical CO_2 reduction with ionic liquids. *Langmuir* **2014**, *30*, 6302−6308.
(14) Brennecke, J. F.; Gurkan, B. Ionic liquids for CO_2 capture and emission reduction. *J. Phys. Chem. Lett.* **2010**, *1*, 3459−3464.
(15) Rosen, B. A.; Salehi-Khojin, A.; Thorson, M. R.; Zhu, W.; Whipple, D. T.; Kenis, P. J. A.; Masel, R. I. Ionic liquid-mediated selective conversion of CO_2 to CO at low overpotentials. *Science* **2011**, *334*, 643−644.
(16) Salehi-Khojin, A.; Jhong, H. R. M.; Rosen, B. A.; Zhu, W.; Ma, S.; Kenis, P. J. A.; Masel, R. I. Nanoparticle silver catalysts that show enhanced activity for carbon dioxide electrolysis. *J. Phys. Chem. C* **2013**, *117*, 1627−1632.
(17) Medina-Ramos, J.; Pupillo, R. C.; Keane, T. P.; Dimeglio, J. L.; Rosenthal, J. Efficient conversion of co_2 to co using tin and other inexpensive and easily prepared post-transition metal catalysts. *J. Am. Chem. Soc.* **2015**, *137*, 5021−5027.
(18) Dimeglio, J. L.; Rosenthal, J. Selective conversion of CO_2 to CO with high efficiency using an inexpensive bismuth-based electrocatalyst. *J. Am. Chem. Soc.* **2013**, *135*, 8798−8801.
(19) Hanc-Scherer, F. A.; Montiel, M. A.; Montiel, V.; Herrero, E.; Sánchez-Sánchez, C. M. Surface structured platinum electrodes for the electrochemical reduction of carbon dioxide in imidazolium based ionic liquids. *Phys. Chem. Chem. Phys.* **2015**, *17*, 23909−23916.
(20) Papasizza, M.; Yang, X.; Cheng, J.; Cuesta, A. Electrocatalytic reduction of CO_2 in neat and water-containing imidazolium-based ionic liquids. *Curr. Opin. Electrochem.* **2020**, *23*, 80−88.
(21) Zhao, S.; Horne, M. D.; Bond, A. M.; Zhang, J. Is the Imidazolium Cation a Unique Promoter for Electrocatalytic Reduction of Carbon Dioxide. *J. Phys. Chem. C* **2016**, *120*, 23989−24001.
(22) Kemna, A.; García Rey, N.; Braunschweig, B. Mechanistic Insights on CO_2 Reduction Reactions at Platinum/[BMIM][BF_4] Interfaces from In Operando Spectroscopy. *ACS Catal.* **2019**, *9*, 6284−6292.
(23) Asadi, M.; Kumar, B.; Behranginia, A.; Rosen, B. A.; Baskin, A.; Repnin, N.; Pisasale, D.; Phillips, P. J.; Zhu, W.; Haasch, R. T.; Klie, R. F.; Kral, P.; Abiade, J. T.; Salehikhojin, A. Robust carbon dioxide reduction on molybdenum disulphide edges. *Nat. Commun.* **2014**, *5*, 4470.
(24) Matsubara, Y.; Grills, D. C.; Kuwahara, Y. Thermodynamic aspects of electrocatalytic co_2 reduction in acetonitrile and with an ionic liquid as solvent or electrolyte. *ACS Catal.* **2015**, *5*, 6440−6452.
(25) Wang, Y.; Hatakeyama, M.; Ogata, K.; Wakabayashi, M.; Jin, F.; Nakamura, S. Activation of CO_2 by ionic liquid EMIM-BF_4 in the electrochemical system: a theoretical study. *Phys. Chem. Chem. Phys.* **2015**, *17*, 23521−23531.
(26) Rey, N. G.; Dlott, D. D. Structural Transition in an ionic liquid controls CO_2 electrochemical reduction. *J. Phys. Chem. C* **2015**, *119*, 20892−20899.
(27) Urushihara, M.; Chan, K.; Shi, C.; Nørskov, J. K. Theoretical study of $EMIM^+$ adsorption on silver electrode surfaces. *J. Phys. Chem. C* **2015**, *119*, 20023−20029.
(28) Neubauer, S. S.; Krause, R. K.; Schmid, B.; Guldi, D. M.; Schmid, G. Overpotentials and faraday efficiencies in co_2 electrocatalysis-the impact of 1-ethyl-3-methylimidazolium trifluoromethanesulfonate. *Adv. Energy Mater.* **2016**, *6*, 1502231.
(29) Tanner, E. E. L.; Batchelor-Mcauley, C.; Compton, R. G. Carbon dioxide reduction in room-temperature ionic liquids: the effect of the choice of electrode material, cation, and anion. *J. Phys. Chem. C* **2016**, *120*, 26442−26447.
(30) Bulut, S.; Eiden, P.; Beichel, W.; Slattery, J. M.; Beyersdorff, T. F.; Schubert, T. J.; Krossing, I. Temperature dependence of the viscosity and conductivity of mildly functionalized and non-functionalized $[Tf_2N]^-$ ionic liquids. *ChemPhysChem* **2011**, *12*, 2296−2310.
(31) Ratschmeier, B.; Kemna, A.; Braunschweig, B. Role of H_2O for CO_2 Reduction Reactions at Platinum/Electrolyte Interfaces in Imidazolium Room-Temperature Ionic Liquids ([EMIM][DCA] and [EMIM][BF_4]). *ChemElectroChem* **2020**, *7*, 1765−1774.
(32) Lagrost, C.; Carrié, D.; Vaultier, M.; Hapiot, P. Reactivities of Some Electrogenerated Organic Cation Radicals in Room-Temperature Ionic Liquids: Toward an Alternative to Volatile Organic Solvents? *J. Phys. Chem. A* **2003**, *107*, 745−752.
(33) Doña Rodríguez, J. M.; Herrera Melián, J. A.; Pérez Peña, J. Determination of the Real Surface Area of Pt Electrodes by Hydrogen Adsorption Using Cyclic Voltammetry. *J. Chem. Educ.* **2000**, *77*, 1195−1197.
(34) Tomita, Y.; Teruya, S.; Koga, O.; Hori, Y. Electrochemical Reduction of Carbon Dioxide at a Platinum Electrode in Acetonitrile-Water Mixtures. *J. Electrochem. Soc.* **2000**, *147*, 4164−4167.
(35) Frisch, M. J.; Trucks, G. W.; Schlegel, H. B.; Scuseria, G. E.; et al. *Gaussian 09*, revision B.01; Gaussian, Inc.: Wallingford, CT, 2009.
(36) Cances, E.; Mennucci, B.; Tomasi, J. A new integral equation formalism for the polarizable continuum model: Theoretical background and applications to isotropic and anisotropic dielectrics. *J. Chem. Phys.* **1997**, *107*, 3032−3041.
(37) Lane, G. H. Electrochemical reduction mechanisms and stabilities of some cation types used in ionic liquids and other organic salts. *Electrochim. Acta* **2012**, *83*, 513−528.
(38) Navarrosuarez, A. M.; Hidalgoacosta, J. C.; Fadini, L.; Feliu, J. M.; Suarezherrera, M. F. Electrochemical oxidation of hydrogen on

https://dx.doi.org/10.1021/acs.jpcc.0c06065
J. Phys. Chem. C 2020, 124, 26094−26105

basal plane platinum electrodes in imidazolium ionic liquids. *J. Phys. Chem. C* **2011**, *115*, 11147−11155.
(39) Feroci, M.; Chiarotto, I.; Ciprioti, S. V.; Inesi, A. On the reactivity and stability of electrogenerated n-heterocyclic carbene in parent 1-butyl-3-methyl-1h-imidazolium tetrafluoroborate: formation and use of n-heterocyclic carbene-co$_2$ adduct as latent catalyst. *Electrochim. Acta* **2013**, *109*, 95−101.
(40) Ooka, H.; Figueiredo, M. C.; Koper, M. T. M. Competition between Hydrogen Evolution and Carbon Dioxide Reduction on Copper Electrodes in Mildly Acidic Media. *Langmuir* **2017**, *33*, 9307−9313.
(41) Rosen, B. A.; Haan, J. L.; Mukherjee, P.; Braunschweig, B.; Zhu, W.; Salehi-Khojin, A.; Dlott, D. D.; Masel, R. I. In situ spectroscopic examination of a low overpotential pathway for carbon dioxide conversion to carbon monoxide. *J. Phys. Chem. C* **2012**, *116*, 15307−15312.
(42) Mei, K.; He, X.; Chen, K.; Zhou, X.; Li, H.; Wang, C. Highly efficient CO_2 capture by imidazolium ionic liquids through a reduction in the formation of the carbene-CO_2 complex. *Ind. Eng. Chem. Res.* **2017**, *56*, 8066−8072.
(43) Feroci, M.; Chiarotto, I.; Forte, G.; Inesi, A. An electrochemical methodology for the cyclic CO_2 "catch and release". The role of the electrogenerated n-heterocyclic carbene in BMIm-BF_4. *J. CO2 Util.* **2013**, *2*, 29−34.
(44) Feroci, M.; Chiarotto, I.; Forte, G.; Vecchio Ciprioti, S.; Inesi, A. Stability and CO_2 capture ability of electrogenerated n-heterocyclic carbene in parent 1-butyl-3-methylimidazoliun ionic liquid (BMIm-X): the role of X^-. *ChemElectroChem* **2014**, *1*, 1407−1414.
(45) Zhou, H.; Zhang, W.-Z.; Liu, C.-H.; Qu, J.-P.; Lu, X.-B. CO_2 adducts of n-heterocyclic carbenes: thermal stability and catalytic activity toward the coupling of CO_2 with epoxides. *J. Org. Chem.* **2008**, *73*, 8039−8044.
(46) Schneider, J.; Jia, H.; Muckerman, J. T.; Fujita, E. Thermodynamics and kinetics of CO_2, CO, and H^+ binding to the metal centre of CO_2 reduction catalysts. *Chem. Soc. Rev.* **2012**, *41*, 2036−2051.
(47) Hoshi, N.; Hori, Y. Electrochemical reduction of carbon dioxide at a series of platinum single crystal electrodes. *Electrochim. Acta* **2000**, *45*, 4263−4270.
(48) Tang, Y.; Liu, X.; McMahan, J.; Kumar, A.; Khan, A.; Sevilla, M.; Zeng, X. Adsorption and Electrochemistry of Carbon Monoxide at the Ionic Liquid-Pt Interface. *J. Phys. Chem. B* **2019**, *123*, 4726−4734.
(49) Chen, Y.; Kanan, M. W. Tin oxide dependence of the co$_2$ reduction efficiency on tin electrodes and enhanced activity for tin/tin oxide thin-film catalysts. *J. Am. Chem. Soc.* **2012**, *134*, 1986−1989.
(50) Cao, Z.; Derrick, J. S.; Xu, J.; Gao, R.; Gong, M.; Nichols, E. M.; Smith, P.; Liu, X.; Wen, X.; Coperet, C.; Chang, C. Chelating N-Heterocyclic carbene ligands enable tuning of electrocatalytic CO_2 reduction to formate and carbon monoxide: surface organometallic chemistry. *Angew. Chem.* **2018**, *130*, 5075−5079.
(51) Eliezer, G. *Electrode Kinetics for Chemists, Chemical Engineers and Materials Scientists*; VCH, 1993.
(52) Fedorov, M. V.; Kornyshev, A. A. Ionic liquids at electrified interfaces. *Chem. Rev.* **2014**, *114*, 2978−3036.
(53) Bockris, J. O'M.; Reddy, A. K. N.; Gamboa-Aldeco, M. E. *Modern Electrochemistry 2A: Fundamentals of Electrodics*, 2nd ed.; Plenum: New York, 2000; Vol. 2A.
(54) Lockett, V.; Sedev, R.; Ralston, J.; Horne, M.; Rodopoulos, T. Differential capacitance of the electrical double layer in imidazolium-based ionic liquids: influence of potential, cation size, and temperature. *J. Phys. Chem. C* **2008**, *112*, 7486−7495.
(55) Pizio, O.; Sokolowski, S.; Sokolowska, Z. Electric double layer capacitance of restricted primitive model for an ionic fluid in slit-like nanopores: A density functional approach. *J. Chem. Phys.* **2012**, *137*, 234705.
(56) Holovko, M.; Kapko, V.; Henderson, D.; Boda, D. On the influence of ionic association on the capacitance of an electrical double layer. *Chem. Phys. Lett.* **2001**, *341*, 363−368.
(57) Boda, D.; Henderson, D.; Chan, K.-Y.; Wasan, D. T. Low temperature anomalies in the properties of the electrochemical interface. *Chem. Phys. Lett.* **1999**, *308*, 473−478.
(58) Cammarata, L.; Kazarian, S.; Salter, P.; Welton, T. Molecular states of water in room temperature ionic liquids. *Phys. Chem. Chem. Phys.* **2001**, *3*, 5192−5200.
(59) Bi, S.; Wang, R.; Liu, S.; Yan, J.; Mao, B.; Kornyshev, A. A.; Feng, G. Minimizing the electrosorption of water from humid ionic liquids on electrodes. *Nat. Commun.* **2018**, *9*, 5222.
(60) Kemna, A.; Braunschweig, B. Potential-Induced Adsorption and Structuring of Water at the Pt(111) Electrode Surface in Contact with an Ionic Liquid. *J. Phys. Chem. Lett.* **2020**, *11*, 7116−7121.
(61) Feng, G.; Jiang, X.; Qiao, R.; Kornyshev, A. A. Water in Ionic Liquids at Electrified Interfaces: The Anatomy of Electrosorption. *ACS Nano* **2014**, *8*, 11685−11694.
(62) Koga, K.; Tanaka, H.; Zeng, X. C. First-order transition in confined water between high-density liquid and low-density amorphous phases. *Nature* **2000**, *408*, 564−567.
(63) Klähn, M.; Seduraman, A. What Determines CO_2 Solubility in Ionic Liquids? A Molecular Simulation Study. *J. Phys. Chem. B* **2015**, *119*, 10066−10078.
(64) Kobayashi, T.; Kemna, A.; Fyta, M.; Braunschweig, B.; Smiatek, J. Aqueous Mixtures of Room-Temperature Ionic Liquids: Entropy-Driven Accumulation of Water Molecules at Interfaces. *J. Phys. Chem. C* **2019**, *123*, 13795−13803.
(65) Huang, M.; Jiang, Y.; Sasisanker, P.; Driver, G. W.; Weingartner, H. Static relative dielectric permittivities of ionic liquids at 25 °C. *J. Chem. Eng. Data* **2011**, *56*, 1494−1499.
(66) Salomonsson, A.; Eriksson, M.; Dannetun, H. Hydrogen interaction with platinum and palladium metal-insulator-semiconductor devices. *J. Appl. Phys.* **2005**, *98*, 014505.

https://dx.doi.org/10.1021/acs.jpcc.0c06065
J. Phys. Chem. C 2020, 124, 26094−26105